PCCP

Cite this: *Phys. Chem. Chem. Phys.*, 2012, **14**, 15458–15463

www.rsc.org/pccp

PAPER

The quantum free energy barrier for hydrogen vacancy diffusion in Na_3AlH_6

Adolfo Poma,[a] Michele Monteferrante,[a] Sara Bonella*[b] and Giovanni Ciccotti[bc]

Received 24th July 2012, Accepted 17th September 2012
DOI: 10.1039/c2cp42536j

The path integral single sweep method is used to assess quantum effects on the free energy barrier for hydrogen vacancy diffusion in a defective Na_3AlH_6 crystal. This process has been investigated *via* experiments and simulations due to its potential relevance in the H release mechanism in sodium alanates, prototypical materials for solid state hydrogen storage. Previous computational studies, which used density functional methods for the electronic structure, were restricted to a classical treatment of the nuclear degrees of freedom. We show that, although they do not change the qualitative picture of the process, nuclear quantum effects reduce the free energy barrier height by about 18% with respect to the classical calculation improving agreement with available neutron scattering data.

1. Introduction

Sodium alanates have been extensively investigated, in experiments[1–4] and simulations,[5–10] because they are considered prototypical systems for solid state hydrogen storage. Palumbo *et al.*,[11,12] in particular, first detected an activated mobility process triggered during the dissociation reaction

$$3NaAlH_4 \Leftrightarrow Na_3AlH_6 + 2Al + 3H_2 \qquad (1)$$

which has attracted considerable interest. They measured the activation barrier to mobility, $\Delta F_{ex} = 0.126$ eV, but could not identify the microscopic species moving in the sample. Several calculations – and further experiments – have been performed to identify this species and three hypotheses have been put forward. Two attribute the signal to the presence of H defects in the sample, most likely in the Na_3AlH_6 crystal formed in the reaction. These are the so-called "local" and "non-local" vacancy diffusions corresponding, respectively, to the rearrangement of the hydrogens around a defective AlH_{6-x} group and to the exchange of an H vacancy between a fully hexacoordinated aluminium and a defective group. The third hypothesis assigns the barrier to the diffusion of a sodium vacancy. Focusing on computational results, Voss and co-workers[13] and Wang *et al.*[14] used the Nudged Elastic Band method[15–17] (NEB) to compute potential energy barriers for these processes. In these calculations, they found considerable barriers for the H related mobility: $\Delta V_l \approx 0.4$ eV and $\Delta V_{nl} \approx 0.75$ eV for the local and non-local processes, respectively. Voss *et al.*[13] also performed neutron scattering experiments on Na_3AlH_6 and determined that there is a hydrogen related diffusion with activation barrier equal to $\Delta F_{ns} = 0.37$ eV. They associated this barrier with local H diffusion, and the signal observed *via* anelastic scattering by Palumbo and co-workers to sodium vacancy mobility. On the other hand, we[18,19] recently investigated the hydrogen vacancy diffusion processes using the single sweep[20] method for free energy reconstruction. Our results show no appreciable free energy barrier for the local diffusion, while we find an activation barrier of $\Delta F = 0.4$ eV for the non-local process. We then attribute to this process the barrier associated with the neutron scattering experiment. The different outcomes of the calculations† leave the identity of the mobile species observed *via* anelastic scattering unresolved and suggest that more work is necessary. In particular, in spite of growing evidence that, contrary to what hypothesized by Palumbo and co-authors, the 0.126 eV barrier cannot originate from processes related to H vacancy diffusion, there is still one point to investigate before these processes can be conclusively ruled out: the relevance of quantum nuclear effects. Both the potential and free energy calculations carried out so far, in fact, used *ab initio* molecular dynamics in which the density functional theory (DFT) description of the electronic structure was combined with the classical treatment of the nuclear degrees of freedom. However, it is well documented that phenomena involving hydrogen can show significant nuclear quantum behavior also at the relatively high temperature of these calculations ($T = 380$ K in our previous work, NEB is, by construction, at zero temperature).

[a] *Dipartimento di Fisica Università "La Sapienza", P.le A. Moro 5, 00185 Roma, Italy. Fax: +39 0649 57697; Tel: +39 4969 4282*
[b] *Dipartimento di Fisica Università "La Sapienza", e CNISM Unità 1, P.le A. Moro 5, 00185 Roma, Italy. E-mail: sara.bonella@roma1.infn.it; Fax: +39 0649 57697; Tel: +39 4991 4208*
[c] *University College Dublin, Room 302b UCD-EMSC, School of Physics, University College Dublin, Belfield, Dublin 4, Ireland*

† These differences are due to the different quantities considered (potential *vs.* free energy) and to the methods used and have been considered elsewhere.[18]

In the gas phase, for example, the intramolecular proton transfer in malonaldehyde shows that, at room temperature, tunneling can reduce the barrier of the reaction by a factor of three or more.[21–24] Quantum effects are also important for hydrogen in solids,[25] where zero point energy is estimated around at least 0.1 eV (non-negligible compared to ambient thermal energy $\approx$0.025 eV). Finally, considering research related to hydrogen storage, recent work[26] has demonstrated the relevance of zero point energy in calculating the enthalpy of formation of hydride $LaNi_5H_7$, a material with significant H capacity and rapid absorption/desorption rate.[27,28] In the following, we will thus reconsider the non-local hydrogen vacancy diffusion in sodium alanates (the only H related process showing activation according to our results), by modifying the free energy calculation performed in ref. 19 so as to account for quantum nuclear effects. This completes the analysis of the previous papers by determining if tunneling and/or zero point energy can lower the calculated free energy barrier to non-local diffusion and make it closer to Palumbo's result, or improve agreement with the neutron scattering. The quantum free energy will be computed using a recently developed method[29] that is summarized in Section 2 (we refer to ref. 29 and the Appendix for some details on its derivation). In Section 3 the simulation setup is described together with the collective variable that we adopted and the results of our calculation are presented and compared with the classical free energy reconstruction.

2. Methods

To obtain the free energy, we will use the quantum single sweep method.[29] This method adapts, *via* minor variations (see Appendix), the single sweep method for classical free energy reconstruction[20] to the quantum case. Its starting point is the path integral[30–32] expression of the quantum free energy of a system of distinguishable particles. In this formalism (see eqn (8) and (9) in the Appendix) the *quantum* free energy, $F(z)$, can be represented as the free energy of a *classical* system in which each quantum particle is represented as a (closed) polymer with P beads‡:

$$F(z) = -\beta^{-1}\ln Q^{-1}\int \mathrm{d}x_1\ldots\mathrm{d}x_P \mathrm{e}^{-\beta U_{\mathrm{eff}}(x_1,\ldots,x_P;\beta)}\delta(\theta(x_1)-z) \quad (2)$$

where $\theta(x) = \{\theta_1(x),\ldots,\theta_\nu(x)\}$ is a set of collective coordinates, $z = \{z_1,\ldots,z_\nu\}$, and $\delta(\theta(x_1)-z) \equiv \prod_{\alpha=1}^{\nu}\delta(\theta_\alpha(x_1)-z_\alpha)$. In the equation above, $Q = \int \mathrm{d}x_1\ldots\mathrm{d}x_P \mathrm{e}^{-\beta U_{\mathrm{eff}}(x_1,\ldots,x_P;\beta)}$ and

$$U_{\mathrm{eff}}(x_1,\ldots,x_P;\beta) = \left[\sum_{i=1}^{P}\frac{1}{2}m\omega_P^2(x_{i+1}-x_i)^2 + \frac{1}{P}\sum_{i=1}^{P}V(x_i)\right] \quad (3)$$

(where $x_{P+1} = x_1$ and $\omega_P = \sqrt{P}/\beta\hbar$).

‡ we use one dimensional notation, but the generalization to more dimensions is straightforward.

To compute eqn (2), single sweep combines an exploration and a reconstruction step. In the exploration step, usually referred to as TAMD[33] (see also ref. 34–36), a set of auxiliary variables $z = \{z_1,\ldots,z_\nu\}$ is introduced. In quantum single sweep, these variables are coupled, *via* the potential $\frac{k}{2}\sum_{\alpha=1}^{\nu}(\theta_\alpha(x_1)-z_\alpha)^2$, to the coordinates of the physical system. The auxiliary variables are thermostated at a temperature $\bar{T}$ higher than the temperature of the system, T, and a "mass" M is assigned to them. Sampling of the extended phase-space is then performed *via* the system of equations

$$\begin{cases} m\ddot{x}_1 = -\nabla_{x_1}U_{\mathrm{eff}}(x;\beta) - k\sum_{\alpha=1}^{\nu}(\theta_\alpha(x_1)-z_\alpha)\nabla_{x_1}\theta_\alpha(x_1) + \mathrm{Therm}(\beta) & \\ m\ddot{x}_i = -\nabla_{x_i}U_{\mathrm{eff}}(x;\beta) + \mathrm{Therm}(\beta) & i = 2,\ldots,P \\ M\ddot{z}_\alpha = k(\theta_\alpha(x_1)-z_\alpha) + \mathrm{Therm}(\bar{\beta}) & \alpha = 1,\ldots,\nu \end{cases}$$

where $x = \{x_1,\ldots,x_P\}$ and $\mathrm{Therm}(\beta)$ indicates coupling to a thermostat at $\beta = 1/k_BT$. If, by an appropriate choice of M and of the thermostat's parameters, adiabatic separation of the x and z motions is induced (making the z much slower than the x), it can be shown[37,38] that the z evolve according to an average force that, in the limit $k \to \infty$, tends to the gradient of the exact quantum free energy of the physical system (see eqn (12) and (13) and discussion in the Appendix). If $\bar{T}$ is high enough, this free energy can be explored quite efficiently even if there are metastabilities. In the second single sweep step, the free energy is reconstructed by interpolation. First, points (centers) along the trajectory of the extended system are used to construct a (irregular) grid in the z space: the first center is the initial position of the z variables, and a new center is deposed when the z-trajectory visits a point farther than a prefixed threshold, d, from all previously generated centers. Second, the free energy is expressed as a linear combination of Gaussians centered on the grid points $\{z_j\}$

$$\tilde{F}(z) = \sum_{j=1}^{J}a_j\mathrm{e}^{-\frac{(z-z_j)^2}{2\sigma^2}} + C, \quad (4)$$

where C is an additive constant, J is the number of grid points, and $a = \{a_j\}$, $\sigma > 0$ are adjustable parameters. The optimal parameters are determined by minimizing (as described in ref. 20 and 39) the objective function

$$E_{\mathrm{r}}(a,\sigma) = \sum_{j=1}^{J}\sum_{\alpha=1}^{\nu}\varepsilon_{j\alpha}\left[f_{j\alpha} + \left(\frac{\partial\tilde{F}(z)}{\partial z_\alpha}\right)_{z=z_j}\right]^2 \quad (5)$$

where $f_{j\alpha}$ is the α component of the mean force computed at $z = z_j$ using

$$f_j = \lim_{\tau\to\infty}\frac{k}{\tau}\int_0^\tau(\theta(\bar{x}_1(t)) - z_j)\mathrm{d}t \quad (6)$$

$(\bar{x}_1(t))$ is a trajectory obtained by propagating the first two equations in the system above with fixed z. Following Monteferrante *et al.*,[39] in eqn (5) we set $\varepsilon_{j\alpha} = 1/|f_{j\alpha}|^2$.

3. Results

To study the quantum effects on the non-local diffusion free energy barrier we used a simulation setup very similar to the

one adopted in the classical calculations.[13,18,19] The microscopic picture that we associate with the non-local diffusion process is quite simple: a pair of Al units is selected in the crystal (one of the units hosts the vacancy) and the process corresponds to an hydrogen transfer from the fully hexacoordinated to the defective unit. We assume that the H transferring from the AlH_6^{3-} to the defective Al group is always the one closer to the acceptor alumina.§ The collective variable chosen to represent this transfer is then the same as in ref. 19, where we also demonstrated *via* a committor test[40] that it can safely represent the reaction. This collective variable is defined as the difference among the distances of the selected hydrogen atom and the two Al atoms, thus

$$D(x) = |\vec{x}_{\mathrm{Al}_1} - \vec{x}_{\mathrm{H}}| - |\vec{x}_{\mathrm{H}} - \vec{x}_{\mathrm{Al}_2}| \qquad (7)$$

where $\vec{x}_K$ is the position of atom K. Given the equilibrium distances of the crystal, in the classical case, the hydrogen transfer is characterized by D changing from $D_1 \approx -2.5$ Å (H bound to the first Al) to $D_2 \approx 2.5$ Å (H bound to the second). As we shall see, a similar behavior is found also in the quantum case, where we will consider $D(x_1)$, *i.e.* the function evaluated at the position of bead number 1 for all atoms involved. As discussed in ref. 19, the crystal lattice is such that the transferring H can experience three different environments (differing for the position of the sodium atoms in the region of the hop) depending on the chosen pair of Al, see Fig. 1 (the figure is the same as in ref. 19). The classical calculations showed free energy barriers substantially independent of the specific case. Since we expect this similarity also for the quantum free energy, in this work we will repeat the calculation only for one of them, corresponding to the most symmetric Na configuration (case (a) in the figure).

All calculations were performed using CPMD.[41] The simulation box was constructed starting from the classical representation of the nuclei. We first removed a negatively charged H¶ from a $(2 \times 2 \times 1)$ cell of the Na_3AlH_6 (classical) perfect crystal. With this choice, the cell, shown in Fig. 2, contains 24 Na^+ ions, 7 AlH_6^{3-} non-defective aluminium groups, and 1 AlH_5^{2-}. The initial configuration for the path integral representation of each atom was generated by placing the first bead at the classical position and then sampling directly, using Levy flight,[43] $P - 1$ coordinates for the other beads from the harmonic part of the effective potential,[32] see eqn (3).‖ We found, by computing the value of the average force at a characteristic point for an increasing number of beads (see below), that $P = 16$ beads were sufficient to converge the path integral representation of the nuclei. To perform the electronic structure calculations, the orbitals were expanded in plane waves, with a spherical cut-off of $E_c = 1360$ eV. Only orbitals corresponding to the Γ point were included. DFT was

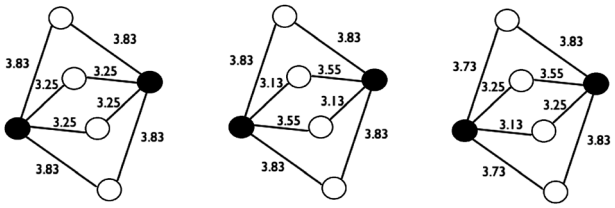

Fig. 1 Positions of the sodium atoms (white circles) around the donor and acceptor alumina (black circles). In all cases, the Na and Al are the vertices of an octahedron. However, while for the (a) configuration, shown in the leftmost panel of the figure, the octahedron is a regular bipyramid and the sodii are in symmetric positions with respect to the line joining the alumina, the other two configurations are less regular and the vertices of the octahedron are distorted, with the largest distortion occurring for the (c) case. The numbers indicate the distances, in Å, between the atoms.

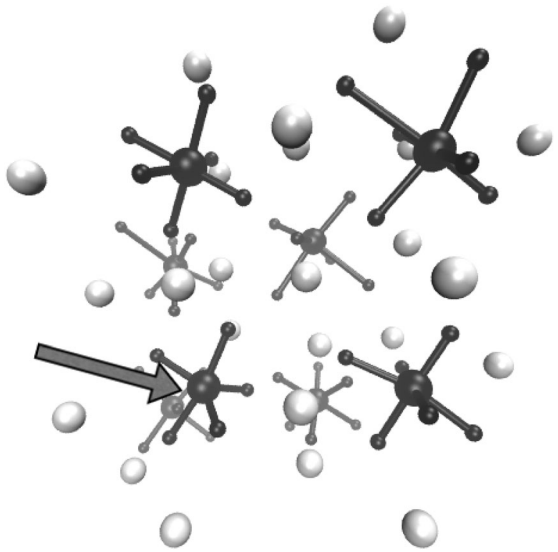

Fig. 2 Snapshot of the simulation box for the defective Na_3AlH_6 crystal. The molecular groups AlH_6^{3-} and AlH_5^{2-} (indicated with the arrow) are shown in black: The Als are the black spheres at the center of the groups, the Hs are the smaller black spheres at the end of the sticks representing the bonds. The Na^+ ions are shown as light gray spheres.

implemented using the BLYP exchange correlation functional[44,45] with generalized gradient approximation. Troullier-Martins pseudopotentials[46] were employed with nine electrons in the valence state of sodium, three electrons in the valence state of Al and one in that of hydrogen. Since we are considering a charged vacancy, the net charge of our system is plus one, thus a background charge was used to eliminate the divergence in the electrostatic energy.[47] The path integral molecular dynamics module of the CPMD code, appropriately modified, was used to propagate the equations of the TAMD system. Due to the considerable cost of path integral *ab initio* MD for a system of this size (the number of nuclear degrees of freedom is $16 \times 3 \times 79 = 3792$) we used Car-Parrinello dynamics[48] to evolve the system. The presence of high nuclear frequencies in the harmonic part of the effective potential U_{eff} made it necessary to use a fictitious mass equal to $m_e = 300$ a.u. for the electronic degrees of freedom to ensure adiabatic separation in the Car-Parrinello dynamics.

§ This is justified based on preliminary, classical, calculations showing that the donor and acceptor Al groups are essentially free to rearrange their hydrogens and rotate so that their relative orientation always favors this particular transfer.

¶ Different analyses[14,19,42] have shown that a positive vacancy is the most likely to appear in the system.

‖ Quantum free particle behavior is assumed in generating this initial condition, subsequent equilibration accounts for the potential interaction, and for possible shifts of the center of mass of the quantum polymer. The procedure is implemented in CPMD *via* the DEBROGLIE keyword.

This value of the mass, somewhat smaller than the one employed in the classical calculations ($m_e \approx 800$ a.u.), required an integration time step $\Delta t = 0.07$ fs (*vs.* $\Delta t = 0.1$ fs in the standard calculation). The nuclear degrees of freedom were kept at a constant temperature $T = 380$ K using a Nosè–Hoover chain with four thermostats, with characteristic frequency $\omega = 15 \times 10^{13}$ s^{-1} (the highest nuclear frequency in the system corresponds to the chain frequency $\omega_P \approx 16 \times 10^{13}$ s^{-1}). To further reduce the cost of our calculations, we did not propagate a TAMD trajectory to set the positions of the centers for the radial basis reconstruction of the free energy (this is in fact not strictly necessary when using only one collective variable). Rather, we selected from the grid used to calculate the classical free energy in ref. 19 a set of 11 points regularly spaced with $D(x) \in [-2.5; 2.5]$ Å (this number of centers proved enough to converge the reconstruction). We then computed the quantum mean forces at these points *via* restrained dynamics (see eqn (6)). In this dynamics we set the (asymptotic) value of the coupling constant between the collective variable and the z equal to $k = 0.5$ a.u. and used a very large value ($M = 10^{12}$ a.u.) for the mass of the fictitious variable. This ensured that the fictitious variables did not move on the time scale necessary to converge the mean force calculation. The restrained trajectories were 5 ps long, 1 ps for equilibration, 4 for average accumulation. This resulted in an relative error of 3% on the calculated mean forces and required about 25 000 hours, using 120 processors on a Linux cluster based on 2-way quad-core Opteron processor (2.1 GHz with 16 GB of RAM) with Infiniband interconnection. 5 ps runs were performed to compute also the classical average forces in ref. 19. As observed in similar cases,[29,49] classical forces showed less fluctuations in the average leading to an error about one order of magnitude smaller. The classical and quantum average forces at the different grid points are shown in Fig. 3 where they are represented as triangles and squares, respectively. The data show differences well outside of the error bars for essentially all points. In particular, the maximum (minimum) value of the classical force is shifted towards larger (smaller) distances by about 0.5 Å with respect to the quantum case. These differences are reflected in the reconstructed free energies reported in Fig. 4, where the classical curve is shown as the black curve with triangles while the quantum result is the curve with squares. The curves in the figure have been shifted to coincide at the leftmost minimum in the classical free energy. The transition state (classical and quantum) is located at the origin, when the transferring proton is equidistant from the Al groups. For the quantum calculations, the transition state is characterized by the first bead at equal distance from the Al groups. The classical free energy profile is slightly asymmetric, with left and right barriers equal to $\Delta F_{Cl} = 0.40$ eV and $\Delta F_{Cr} = 0.45$ eV, respectively. The asymmetry of the quantum result is more pronounced, with the new barriers equal to $\Delta F_{Ql} = 0.33$ eV and $\Delta F_{Qr} = 0.41$ eV. There is also a shift of the minima towards the origin, often observed in calculations of this kind,[21–24,29] and which is usually considered a manifestation of tunneling effects. The difference among the classical and quantum free energy barriers, while detectable, is quite small with the larger discrepancy observed for the left barrier and equal to 0.07 eV. The quantum free energy is in better agreement with the result of the neutron scattering experiment ($\Delta F_{ns} = 0.37$ eV), with a reduction of the barrier of about 18% that we attribute to tunneling (as indicated by the shift of the minima). The calculation presented here improves the agreement with these experiments, but it does not qualitatively change the result of the previous calculation. The data thus confirm that the neutron scattering signal is due to non-local H diffusion, while the signal in anelastic spectroscopy originates elsewhere. The validity of our conclusions relies on two main factors. First of all, we trust the accuracy of the microscopic model adopted (and in particular of the DFT calculation of the electronic structure). This model was tested in ref. 18 by comparing structural properties of the (perfect) crystal with classical nuclei with experimental data[2] and proved satisfactory. Secondly, as with all free energy calculations, our conclusion depends on the choice of the collective variables adopted to describe the process. In particular, we assumed that the H transfer is not assisted by the motion of atoms other than the donor and acceptor Als. For example, then, cooperative motions of the lattice, and the

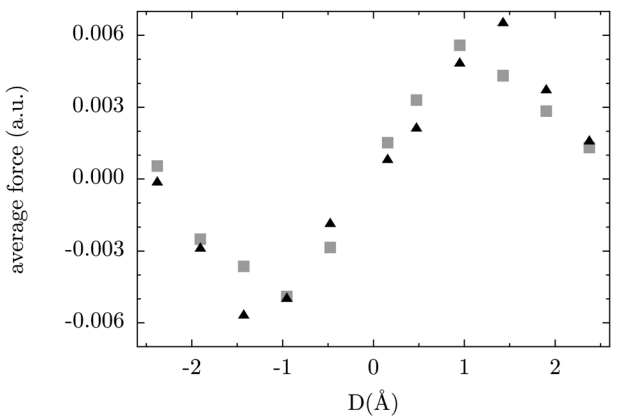

Fig. 3 Classical (triangles) and quantum (squares) average forces. The size of the squares is representative of the error, while the error on the classical calculations is too small to be visible.

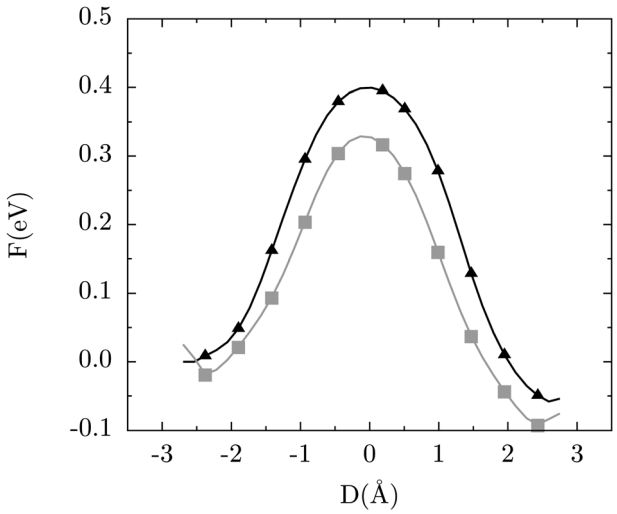

Fig. 4 Classical (black curve with triangle) and quantum (light gray curve with squares) free energies. To set the zero of the free energies to the same value, the curves have been shifted so as to coincide at the leftmost point of the grid.

possible involvement of the Na ions in "shuttling" the transferring hydrogen are not accounted for. This choice, which is the same adopted in all calculations performed on the system, is motivated by direct observation of the transfer in preliminary calculations and supported by the (classical) committor test performed in ref. 40. Having excluded the local and non-local hydrogen transfer process, the most likely hypothesis within the set of processes considered for explaining the signal observed in an elastic scattering seems indeed to be sodium vacancy mobility.

4. Conclusions

In this paper, we used the path integral single sweep method to investigate quantum effects on the free energy barrier for non-local hydrogen diffusion in sodium alanates. We showed that these effects, due most likely to tunneling, cause a reduction of the barrier 0.07 eV for the left barrier and 0.04 eV for the right one. Although this reduction is non-negligible compared to the typical thermal energy, it is not enough to lead to agreement with the experimental signal of Palumbo, $\Delta F_{ex} = 0.126$ eV. On the other hand, the new result is in better agreement with the barrier observed by Voss *et al.*[13] Based on this, we confirm (1) that the non-local H diffusion is the process observed for the neutron scattering experiment and that (2) the signal in anelastic scattering cannot be attributed to either of the H related processes considered so far in the literature. The more likely origin of this signal among current hypothesis is thus the mobility of a sodium vacancy as suggested by the calculation of the potential energy barriers in ref. 13.

5. Appendix

In the following, we discuss in some more detail the quantum single sweep method. Let us start from the definition of the quantum free energy of a system of distinguishable particles. Introducing a set of collective variables $\theta(\hat{x}) = \{\theta_1(\hat{x}),\ldots,\theta_\nu(\hat{x})\}$, assumed to be a function of the coordinate operators of the system, this quantity is given by

$$F(z) = -\beta^{-1} \ln \mathrm{Tr}\left\{\frac{\mathrm{e}^{-\beta\hat{H}}}{Z}\delta(\theta(\hat{x}) - z)\right\} \tag{8}$$

where $z = \{z_1,\ldots,z_\nu\}$, $\delta(\theta(\hat{x}) - z) \equiv \prod_{\alpha=1}^{\nu} \delta(\theta_\alpha(\hat{x}) - z_\alpha)$, and $Z = \mathrm{Tr}\{\mathrm{e}^{-\beta\hat{H}}\}$ is the partition function. Evaluating the trace in the coordinate basis, and using the fact that the collective variables are diagonal in this basis, the free energy can be expressed as

$$\begin{aligned} F(z) &= -\beta^{-1} \ln \frac{1}{Z}\int \mathrm{d}x_1 \langle x_1|\mathrm{e}^{-\beta\hat{H}}\delta(\theta(\hat{x}) - z)|x_1\rangle \\ &= -\beta^{-1} \ln \frac{1}{Z}\int \mathrm{d}x_1 \langle x_1|\mathrm{e}^{-\beta\hat{H}}|x_1\rangle\delta(\theta(x_1) - z) \end{aligned} \tag{9}$$

The matrix element of the Boltzmann operator can be written most conveniently using a path integral representation. This representation is obtained using the steps introduced by Feynman:[30] insert $P-1$ resolutions of the identity in the coordinate representation to write $\langle x_1|\mathrm{e}^{-\beta\hat{H}}|x_1\rangle = \int \mathrm{d}x_2 \ldots \mathrm{d}x_P \prod_{i=1}^{P} \langle x_{i+1}|\mathrm{e}^{-\varepsilon\hat{H}}|x_i\rangle$ (with $\varepsilon = \beta/P$, and $x_{P+1} = x_1$) and then use the Trotter factorization

$$\begin{aligned} \langle x_{i+1}|\mathrm{e}^{-\varepsilon\hat{H}}|x_i\rangle &= \left\langle x_{i+1}\middle|\mathrm{e}^{-\varepsilon\frac{\hat{p}^2}{2m}}\middle|x_i\right\rangle \mathrm{e}^{-\varepsilon[V(x_i)+V(x_i+1)]} \\ &\quad + \mathcal{O}\left(\varepsilon^2\left[\frac{\hat{p}^2}{2m}, V(\hat{x})\right]\right) \\ &\approx \sqrt{\frac{m}{2\pi\varepsilon\hbar^2}}\mathrm{e}^{-\frac{m(x_{i+1}-x_i)^2}{2\varepsilon\hbar^2}}\mathrm{e}^{-\varepsilon[V(x_i)+V(x_i+1)]} \end{aligned} \tag{10}$$

to approximate each matrix element in the product over i. Using these two steps in eqn (9), the free energy becomes

$$\begin{aligned} F(z) \approx -\beta^{-1} \ln Q^{-1} \int \mathrm{d}x_1 \ldots \mathrm{d}x_P \mathrm{e}^{-\sum_{i=1}^{P}\frac{m(x_{i+1}-x_i)^2}{2\varepsilon\hbar^2}} \mathrm{e}^{-\varepsilon\sum_{i=1}^{P}V(x_i)} \\ \times \delta(\theta(x_1) - z) \end{aligned} \tag{11}$$

where we indicated with Q the path integral representation of the partition function. The expression above becomes exact for $P \to \infty$. If now introduce the "chain frequency" $\omega_P = \sqrt{P}/\beta\hbar$ and the effective potential defined in eqn (3), we obtain the expression in eqn (2). The harmonic terms in the effective potential represent the quantum kinetic energy and link the different beads of the polymer, each feeling the Pth fraction of the potential V which describes the external and/or interaction potential (for many particle systems). As a direct consequence of eqn (9), in this free energy the delta function constraining the collective variables at the value z acts only on the first bead of the polymer. Essentially all the classical schemes available for free energy calculation can be adapted to this expression. As mentioned in the text, we focused on single sweep.[20] The quantum version of the method is obtained by retracing very closely the steps of the original derivation. In the following, we highlight the differences between the quantum and classical cases, but rely on the original references for the details of the proofs when these differences do not introduce significant changes. In particular, we will address only the exploration step (*i.e.* the TAMD part of single sweep), since the reconstruction *via* the Gaussian basis set is essentially identical to the classical procedure. The main difference between classical and quantum TAMD is in the definition of the potential coupling physical and fictitious variables. In classical single sweep, the "full" particle is coupled to the auxiliary variable: if we indicate with $\boldsymbol{r} = \{r_1,\ldots,r_n\}$ the Cartesian coordinates of the classical system of n particles (with $r_i = (r_{ix},r_{iy},r_{iz})$), the coupling is $\frac{k}{2}\sum_{\alpha=1}^{\nu}(\theta_\alpha(\mathbf{r}) - z_\alpha)^2$, see, for example, eqn (8) in ref. 33. For the quantum case, as indicated in the text, this interaction takes the form $\frac{k}{2}\sum_{\alpha=1}^{\nu}(\theta_\alpha(x_1) - z_\alpha)^2$. This coupling affects only the coordinate x_1 in each path integral polymer, so it involves only one of the beads that represent the quantum particle. With this coupling, we can proceed in analogy to the classical single sweep to establish the successive steps of the method, and in particular the evolution defined by the system in Section 2. The most important property of this system is the fact that, in the limits for M, k and the thermostat parameters indicated in the text, the z variables explore the physical free energy thus ensuring that the centers collected along their trajectory are in relevant regions of the z space. This can be

understood by observing that, if the auxiliary variables move much slower than the physical ones, they are subject to an effective force which is given by the average of the right hand side of the third member of the system of equations with respect to the conditional probability for x given z.[37,38] The thermostat is not affected by this average, so the relevant quantity is

$$k\int \mathrm{d}x(\theta_\alpha(x_1)-z_\alpha)\rho(x|z) \qquad (12)$$

where $\rho(x|z)=Q_{\mathrm{k}}^{-1}\mathrm{e}^{-\beta\left[U_{\mathrm{eff}}(x;\beta)+\frac{k}{2}\sum_{\alpha=1}^{\nu}(\theta_\alpha(x_1)-z_\alpha)^2\right]}$ is the conditional probability for x given z (here $Q_{\mathrm{k}}^{-1}=\int \mathrm{d}x\mathrm{e}^{-\beta\left[U_{\mathrm{eff}}(x;\beta)+\frac{k}{2}\sum_{\alpha=1}^{\nu}(\theta_\alpha(x)-z_\alpha)^2\right]}$). Let us now define

$$F_k(z)=-\beta^{-1}\ln \mathcal{Q}_k^{-1}\int \mathrm{d}x\mathrm{e}^{-\beta U_{\mathrm{eff}}(x;\beta)}\mathrm{e}^{-\frac{\beta k}{2}\sum_{\alpha=1}^{\nu}(\theta_\alpha(x_1)-z_\alpha)^2} \qquad (13)$$

with $\mathcal{Q}_k^{-1}=\int \mathrm{d}x\mathrm{d}z\mathrm{e}^{-\beta\left[U_{\mathrm{eff}}(x;\beta)+\frac{k}{2}\sum_{\alpha=1}^{\nu}(\theta_\alpha(x_1)-z_\alpha)^2\right]}$. The average force is given by $\nabla_z F_k(z)$. In the limit $k\to\infty$, the product of Gaussians in the equation above becomes a product of delta functions and the path integral form of the quantum free energy, see (2), is recovered.

Acknowledgements

The authors thank R. Vuilleumier for useful discussions. Funding from the IIT SEED project SIMBEDD and from the SFI Grant 08-IN.1-I1869 is acknowledged. The calculations were performed on the Matrix cluster at CASPUR with the support of a Standard HPC-Grant 2012.

References

1 B. Bogdanovi and M. Schwickardi, *J. Alloys Compd.*, 1997, **1**, 253.
2 E. Ronnebro, D. Noreus, K. Kadir, A. Reiser and B. Bogdanovic, *J. Alloys Compd.*, 2000, **299**, 101.
3 G. Sandrock, K. Gross and G. Thomas, *J. Alloys Compd.*, 2002, **339**, 299.
4 B. Yebka and G. Nari, *Mater. Res. Soc. Symp. Proc.*, 2003, **801**, BB4.4.
5 A. Peles, J. A. Alford, Z. Ma, L. Yang and M. Y. Chou, *Phys. Rev. B: Condens. Matter Mater. Phys.*, 2004, **70**, 165105.
6 S. Li, P. Jena and R. Ahuja, *Phys. Rev. B: Condens. Matter Mater. Phys.*, 2006, **73**, 214107.
7 B. Kiran, A. K. Kandalam and P. Jena, *J. Chem. Phys.*, 2006, **124**, 224703.
8 B. Kiran, P. Jena, X. Li, A. Grubisic, S. T. Stokes, G. F. Gantefor, K. H. Bowen, R. Burgert and H. Schnockel, *Phys. Rev. Lett.*, 2007, **98**, 256802.
9 X. Ke and I. Tanaka, *Phys. Rev. B: Condens. Matter Mater. Phys.*, 2005, **71**, 024117.
10 C. Araujo, S. Li, R. Ahuja and P. Jena, *Phys. Rev. B: Condens. Matter Mater. Phys.*, 2005, **72**, 165101.
11 O. Palumbo, R. Cantelli, A. Paolone, C. Jensen and S. Srinivasan, *J. Phys. Chem. B*, 2005, **109**, 1168.
12 O. Palumbo, A. Paolone, R. Cantelli, C. Jensen and M. Sulic, *J. Phys. Chem. B*, 2006, **110**, 9105.
13 J. Voss, Q. Shi, H. Jacobsen, M. Zamponi, K. Lefmann and T. Vegge, *J. Phys. Chem. B*, 2007, **111**, 3886.
14 J. Wang, Y. Du, H. Xu, L. Sun and Z. Liu, *Appl. Phys. Lett.*, 2009, **95**, 111910.
15 G. Mills and H. Jonsson, *Phys. Rev. Lett.*, 1994, **72**, 1124.
16 H. Jonsson, G. Mills and K. Jacobsen, *Classical and quantum dynamics in the condensed phase*, World Scientific, Singapore, 1998, p. 385.
17 G. Henkelman, B. P. Uberuaga and H. Jonsson, *J. Chem. Phys.*, 2000, **113**, 9901.
18 M. Monteferrante, S. Bonella, S. Meloni, E. Vanden-Eijnden and G. Ciccotti, *Sci. Model. Simul.*, 2008, **15**, 187.
19 M. Monteferrante, S. Bonella and G. Ciccotti, *Phys. Chem. Chem. Phys.*, 2011, **13**, 10546.
20 L. Maragliano and E. Vanden-Eijnden, *J. Chem. Phys.*, 2008, **128**, 184110.
21 K. F. Wong, J. L. Sonnenberg, F. Paesani, T. Yamamoto, J. Vaníček, W. Zhang, H. B. Schlegel, D. A. Case, T. E. Cheatham, W. H. Miller and G. A. Voth, *J. Chem. Theory Comput.*, 2010, **6**, 2566.
22 R. Iftimie and J. Schofield, *J. Chem. Phys.*, 2001, **114**, 6763.
23 R. Iftimie and J. Schofield, *J. Chem. Phys.*, 2001, **115**, 5891.
24 M. E. Tuckerman and D. Marx, *Phys. Rev. Lett.*, 2001, **86**, 4946.
25 S. Tsuneyuki, *Curr. Opin. Solid State Mater. Sci.*, 2002, **6**, 147.
26 T. Kaneko, A. Tezuka, H. Ogawa and T. Ikeshoji, *J. Chem. Phys.*, 2011, **110**, 063533.
27 J. van Vucht, F. Kujipers and H. C. A. M. Burning, *Philips Res. Rep.*, 1970, **25**, 133.
28 J. Willems and K. Buschow, *J. Less-Common Met.*, 1987, **129**, 13.
29 S. Bonella and R. Vuilleumier, *submitted to Journal of Chemical Theory and Computation*.
30 R. P. Feynman and A. R. Hibbs, *Quantum Mechanics and Path Integrals*, McGraw-Hill, 1965.
31 M. E. Tuckerman, *Statistical mechanics: Theory and molecular simulation*, Oxford University Press, Oxford, 2010.
32 M. E. Tuckerman, D. Marx, M. Klein and M. Parrinello, *J. Chem. Phys.*, 1996, **104**, 5579.
33 L. Maragliano and E. Vanden-Eijnden, *Chem. Phys. Lett.*, 2006, **426**, 168.
34 L. Rosso, P. Minary, M. Zhu and Z. Tuckerman, *J. Chem. Phys.*, 2002, **116**, 4389.
35 J. Abrams and M. Tuckerman, *J. Phys. Chem. B*, 2008, **112**, 15742.
36 J. VandeVondele and U. Rothlisberger, *J. Phys. Chem. B*, 2002, **106**, 203.
37 A. Bensoussau, J.-L. Lions and G. Papanicolau, *Asymptotic analysis for periodic structures*, North Holland, New York, 1978.
38 E. Vanden-Eijnden, *Continuum*, 2003, **1**, 385.
39 M. Monteferrante, S. Bonella, S. Meloni and G. Ciccotti, *Mol. Simul.*, 2009, **35**, 1116.
40 L. Maragliano, A. Fischer, E. Vanden-Eijnden and G. Ciccotti, *J. Chem. Phys.*, 2006, **125**, 024106.
41 CPMD, Copyright IBM Corp. 1999–2001, Copyright MPI für Festkorperforshung Stittgart 1997–2004.
42 S. Hao and D. S. Sholl, *Appl. Phys. Lett.*, 2008, **93**, 251901.
43 L. D. Fosdick and H. F. Jordan, *Phys. Rev.*, 1966, **143**, 58.
44 A. D. Becke, *Phys. Rev. A*, 1988, **38**, 3098.
45 C. Lee, W. Yang and R. Parr, *Phys. Rev. B: Condens. Matter Mater. Phys.*, 1988, **37**, 785.
46 N. Troullier and J. L. Martins, *Phys. Rev. B: Condens. Matter Mater. Phys.*, 1991, **43**, 1993.
47 G. Makov and M. C. Payne, *Phys. Rev. B: Condens. Matter Mater. Phys.*, 1995, **51**, 4014.
48 R. Car and M. Parrinello, *Phys. Rev. Lett.*, 1985, **55**, 2471.
49 D. Laria, G. Ciccotti, M. Ferrario and R. Kapral, *Chem. Phys.*, 1994, **180**, 181.